

PAPER

Enhanced electron acceleration in aligned nanowire arrays irradiated at highly relativistic intensities

To cite this article: A Moreau *et al* 2020 *Plasma Phys. Control. Fusion* **62** 014013

View the [article online](#) for updates and enhancements.





IOP | ebooksTM

Bringing you innovative digital publishing with leading voices to create your essential collection of books in STEM research.

Start exploring the collection - download the first chapter of every title for free.

Enhanced electron acceleration in aligned nanowire arrays irradiated at highly relativistic intensities

A Moreau¹ , R Hollinger¹, C Calvi², S Wang¹, Y Wang¹, M G Capeluto^{1,3} ,
A Rockwood², A Curtis², S Kasdorf¹, V N Shlyaptsev¹, V Kaymak⁴,
A Pukhov⁴ and J J Rocca^{1,2,5}

¹Electrical and Computer Engineering Department, Colorado State University, Fort Collins, CO 80523, United States of America

²Physics Department, Colorado State University, Fort Collins, CO 80523, United States of America

³Departamento de Física, Universidad de Buenos Aires, Ciudad Universitaria, 1428 Buenos Aires, Argentina

⁴Institut für Theoretische Physik 1, Heinrich-Heine-Universität Düsseldorf, D-40225 Düsseldorf, Germany

E-mail: afmoreau@colostate.edu and jorge.rocca@colostate.edu

Received 26 July 2019, revised 17 September 2019

Accepted for publication 11 October 2019

Published 1 November 2019



CrossMark

Abstract

We report a significant enhancement in both the energy and the flux of relativistic electrons accelerated by ultra-intense laser pulse irradiation ($>1 \times 10^{21} \text{ W cm}^{-2}$) of near solid density aligned CD_2 nanowire arrays in comparison to those from solid CD_2 foils irradiated with the same laser pulses. Ultrahigh contrast femtosecond laser pulses penetrate deep into the nanowire array creating a large interaction volume. Detailed three dimensional relativistic particle-in-cell simulations show that electrons originating anywhere along the nanowire length are first driven towards the laser to reach a lower density plasma region near the tip of the nanowires, where they are accelerated to the highest energies. Electrons that reach the lower density plasma experience direct laser acceleration up to the dephasing length, where they outrun the laser pulse. This yields an electron beam characterized by a $3\times$ higher electron temperature and an integrated flux $22.4\times$ larger respect to foil targets. Additionally, the generation of $>1 \text{ MeV}$ photons were observed to increase up to $4.5\times$.

Keywords: electron acceleration, laser-matter interactions, x-rays, high energy density plasmas, hot electrons

(Some figures may appear in colour only in the online journal)

1. Introduction

In laser-matter interactions at the highest intensities electrons are rapidly ripped from their parent atoms and accelerated to relativistic energies [1, 2]. The resulting relativistic electron beams in turn drive processes such as heavy ion acceleration [3–5], proton beams [6, 7], positron generation [8–10], and bright x-ray and gamma ray beams [11–14]. All these processes depend upon a high charge, high energy electron distribution, and therefore from the efficient coupling of the laser energy into electrons.

Significant research effort has been devoted to the study of structured target geometries which aim to improve the interaction over solid foil targets. Increased x-ray emission has been observed from gratings [15], ‘smoked’ targets [16, 17], nanowire arrays [14, 17–20] and other structured targets [21–23]. Purvis *et al* demonstrated efficient volumetric heating of aligned nanowires array targets [24] which lead to near solid density plasmas with extreme energy densities and degrees of ionization [25]. Volumetric heating of sub-wavelength diameter metal nanowire targets at intensities up to $\approx 4 \times 10^{19} \text{ W cm}^{-2}$ converted up to 20% of the optical laser energy into $>1 \text{ keV}$ x-rays [26]. Additionally, irradiation of deuterated polyethylene

⁵ Author to whom any correspondence should be addressed.

nanowire arrays at similar intensities achieved $500\times$ enhancement in D-D fusion neutrons [27]. All these results suggest that the use of nanowire targets lead to hotter electron temperatures over much larger volumes driving such effects.

Measurements of the hot electron distribution from structured targets such as carbon nanotubes [28], micro-channel plates [29], wavelength-scale microwires [30–32], and sub-wavelength nanowires [30, 33–35] have all shown enhanced electron heating. While electron acceleration by microchannel plate and microwire targets have been studied at highly relativistic intensities [29, 31], measurements of nanowire array targets have been limited to intensities below $10^{19} \text{ W cm}^{-2}$ [30, 33]. Here we report on the irradiation of near solid density arrays of aligned CD_2 nanowires at highly relativistic intensities $>1 \times 10^{21} \text{ W cm}^{-2}$ and demonstrate a significant enhancement in both the energy and the flux of relativistic electrons as compared with solid density foil targets of the same material. An increase in the flux of MeV photons driven by hot electrons was also observed. Results of three dimensional relativistic particle-in-cell (PIC) simulations that elucidate the process of electron acceleration in these nanowire arrays are also presented.

2. Methods

2.1. Experiment design

The targets utilized in this study consisted of vertically aligned deuterated polyethylene (CD_2) nanowires on a thin CD substrate ($\approx 300\text{--}500 \mu\text{m}$ thick). The nanowires had diameters of 200 nm with lengths of $\approx 5 \mu\text{m}$. The nanowire arrays had an average density 16% of solid density, with an average distance between wires of $\approx 450 \text{ nm}$. The targets were fabricated as described in [27] by heated extrusion into anodic aluminum membranes. The targets were imaged with a scanning electron microscope to ensure acceptable quality. For comparison solid density CD_2 foils targets of the same material were fabricated using a hydraulic press and measured to be also $500 \mu\text{m}$ thick.

The experiment was conducted on the ALEPH 400 laser at Colorado State University's Advanced Beam Laboratory. The ALEPH 400 is a petawatt-class Ti:Sapphire laser delivering 800 nm pulses which are frequency doubled to $\lambda = 400 \text{ nm}$ by a 0.8 mm thick type 1 KDP crystal. This allows for a contrast $>1 \times 10^{12}$ [36]. The ultrahigh contrast was required to prevent a pre-plasma from prematurely closing the gap between the wires prior to the arrival of the main pulse. In this experiment the pulses duration was 45 fs FWHM and beam was focused by an $F/2$ off-axis parabola to a focal spot $\approx 1.6 \mu\text{m}$ full width at half maximum, with pulse energies ranging from 10 to 11 J , yielding intensities on target up to $2.7 \times 10^{21} \text{ W cm}^{-2}$. Target plane alignment was achieved by imaging the target surface on every shot with a $20\times$ microscope set to image the laser focus, ensuring peak intensity on target. Pulses were linearly polarized. The targets were irradiated at normal incidence with the nanowires aligned parallel to the laser propagation direction. In illustration of the experimental setup is shown in figure 1.

2.2. Electron spectrometer

To measure the electron energy a magnetic electron spectrometer was deployed at 30.4 cm from the plasma along the laser forward direction. The collimating entrance of the instrument consists of a $2 \text{ mm} \times 2 \text{ mm}$ square cut into stainless steel plate 1.27 cm thick, collecting $4.3 \times 10^{-5} \text{ Sr}$. No significant change in the collected spectra was observed when the distance from the plasma to the electron spectrometer was increased to 49 cm . The instrument signal was recorded on Fujifilm BAS-MS image plate and was read on a GE Storm scanner calibrated with an ^{55}Fe source by the process described in [37]. Electrons obliquely incident on the image plate deposit energy along a larger path length due to their path projection in the sensitive layer. To prevent over counting of the electrons the dispersion plane is curved such that electrons are incident at near normal to the image plate as shown in figure 1(c). The magnetic field in the center of the gap was measured to be 0.23 T . The instrument was modeled using the 3D simulation software SIMION [38] taking into account the fringing fields. Electron trajectories were calculated and any remaining deviation from normal incidence was corrected for. The energy range of the spectrometer is $0.3\text{--}80 \text{ MeV}$. To enable experiments at repetition rates better than $1 \text{ shot}/2 \text{ min}$ the spectrometer was installed with a pneumatically actuated gate valve in front of the collimator to allow for rapid reloading of a new image plate.

Figure 2 shows measured electron spectra for a series of shots on both solid foil targets and aligned nanowire array targets. Shown with circular markers are five representative shots on a $500 \mu\text{m}$ CD_2 foil target. All data are from single shots. It is noted the electrons with an energy lower than 2 MeV were not detected by the instrument on high intensity shots despite an instrumental range down to 300 keV . This is likely the result of two mechanisms: target charging that can cause refluxing of the low energy electrons [39, 40], and charging of the electron spectrometer pinhole [41].

2.3. High energy x-ray detector

As discussed previously, one application for high charge, relativistic electron beams is the generation of very high energy photons ($>1 \text{ MeV}$) via bremsstrahlung radiation. The efficient generation of MeV photons requires a high-Z converter. However even in the absence of a converter, the substrate that supports the nanowires is sufficiently thick to allow for a small fraction of electrons to radiate via bremsstrahlung. To measure this radiation an EJ-228 plastic scintillator was coupled to a Hamamatsu H2431-50 photomultiplier tube (PMT) biased to 1500 V . The PMT was surrounded by a Pb enclosure with 10 cm of lead on the side facing the plasma and 5 cm of lead on all other sides. The PMT was placed on the plane of the interaction, at 244 cm from TCC and at 45° from the laser beam axis, which also defines the target normal as shown in figure 1(a). Accounting for photon propagation through a 1.2 cm Al flange and the 10 cm of lead the instrument sensitivity peaks at 4 MeV and falls by >2 orders of magnitude below 1 MeV .

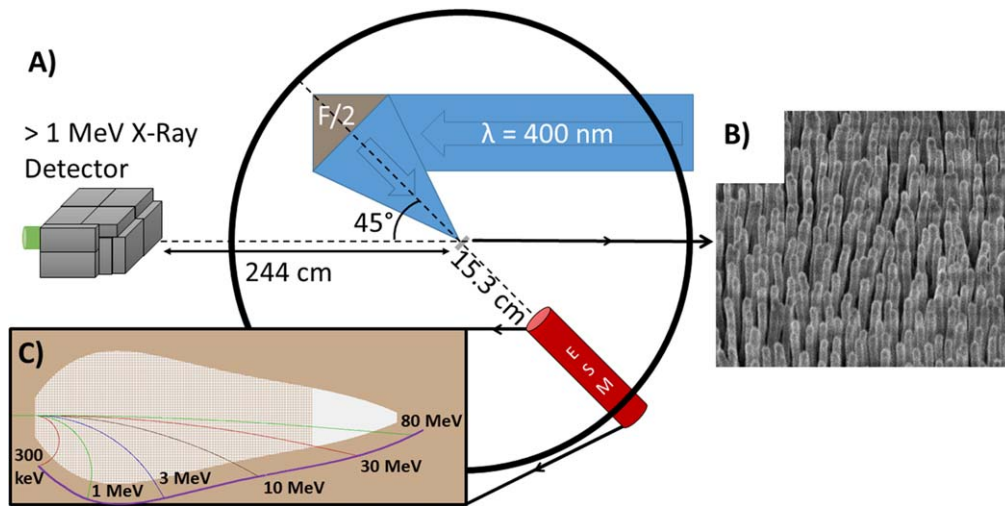


Figure 1. (A) Diagram of the experiment showing the $\lambda = 400$ nm beam focusing onto the target driving hot electron production in the laser forward direction where it is collected by the electron spectrometer (ESM) on the laser axis. Also shown is the MeV photon detector inside of a lead enclosure at 45° from the target normal direction. (B) Scanning electron microscope image of a CD_2 nanowire array. (C) SIMION simulation of the electron spectrometer showing the path for electrons of various energies. The curved dispersion plane of the BAS-MS image plate is shown by the purple line.

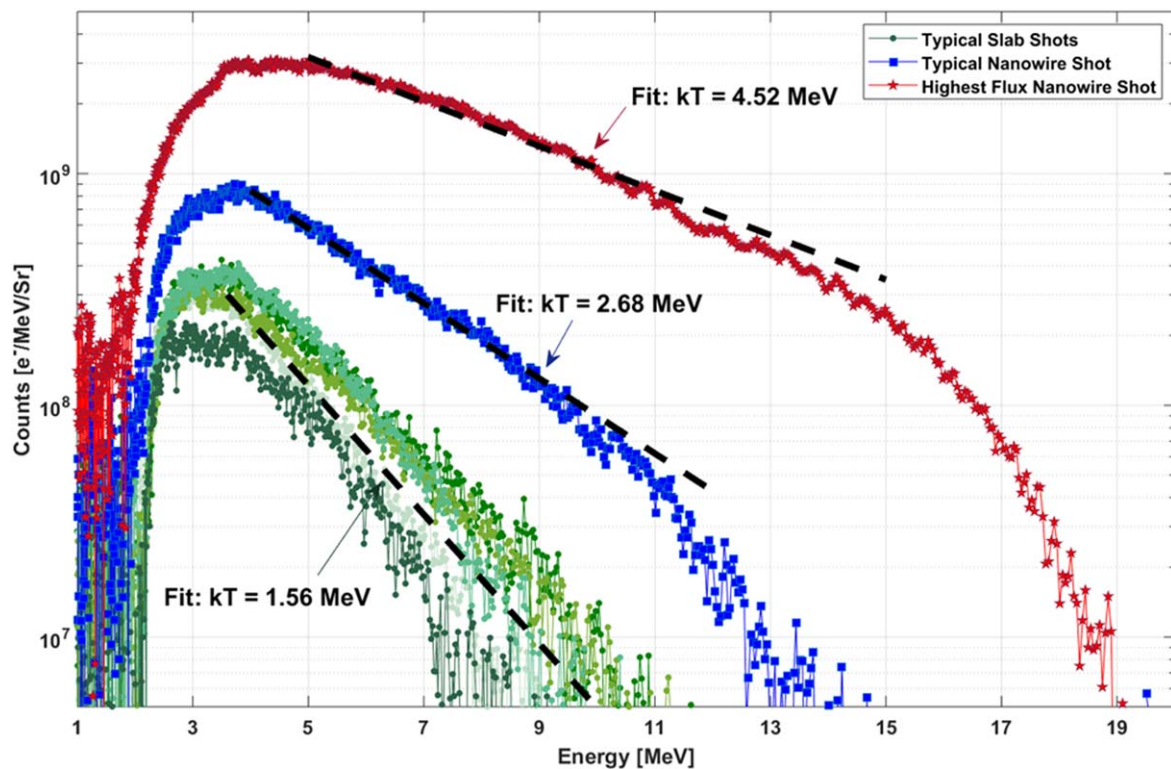


Figure 2. Measured electron spectra for solid foil targets (circles) and nanowire targets (squares and stars). All spectra are single shot, with five shots shown for the case of foil targets, each with a different color shade (color online). The squares show a typical result for nanowire shots while the stars represent the highest temperature and flux shot of the experiment. Shot to shot the variation for nanowire targets occurs due to the random location of wires, resulting in a varying number of wires within the focal spot.

2.4. PIC modeling

PIC simulations were conducted using the fully relativistic three dimensional Virtual Laser Plasma Laboratory code [42]. The code includes packages for optical field ionization (OFI) and binary collisions including electron impact ionization.

The OFI package treated the ionization as an under barrier tunneling phenomenon in the electric field of the laser pulse, only allowing for sequential step ionization. Coulomb collisional probabilities between all particles were calculated by a binary collision package. The simulations considered a

three-dimensional geometry of a single nanowire with the boundary of the simulation in the transverse direction being defined as the midpoint between two wires. The boundaries in the transverse direction were periodic, effectively creating a mirror symmetry in the simulation. The laser field was assumed to correspond to a $\lambda = 400$ nm linearly polarized plane wave with a gaussian time envelope of $a(t) = a_0 \exp\left(-\frac{t^2}{\tau^2}\right)$ with $\tau = 45$ fs FWHM pulse duration impinging on the CD_2 wire at normal incidence. The modeling of a single wire, required by computational efficiency, neglects the spatial variation of the laser beam intensity but is a reasonable approximation. The grid size ranged from $7344 \times 60 \times 60$ to $12\,144 \times 60 \times 60$ and the cell size was $0.0073 \lambda \times 0.017 \lambda \times 0.017 \lambda$. The time step used in the simulation was $0.002\,66$ fs. The simulations were conducted for 200 nm diameter by $5 \mu\text{m}$ length CD_2 wires at 19% of solid density (wire to wire distance of 406 nm) irradiated with an $\lambda = 400$ nm laser pulses at an intensity of $4 \times 10^{21} \text{ W cm}^{-2}$ corresponding to $a_0 = 21.6$ ($a_0 = \lambda [\mu\text{m}] \sqrt{\frac{\text{Laser Intensity} [\text{Wcm}^{-2}]}{1.37 \times 10^{18}}}$). A post processor code was developed to visualize the electron trajectories and collect synthetic spectra for the electrons.

3. Results and discussion

Figure 2 shows measured electron spectra for a series of shots on both solid foil targets and aligned nanowire array targets. The data represented by circles correspond to 5 separate shots on a foil target, each identified with a different shade of green. When the measured high energy tail in the electron distribution is fit with an exponential to yield an electron temperature for the high energy electrons, the value for the foil targets is found to be 1.56 ± 0.06 MeV. The $(I\lambda^2)^{1/3}$ scaling proposed by Beg *et al* [43] predicts a $T_{\text{hot}} = 1.62$ MeV, value that is within the error bars of our measurement. More recent scaling proposed by Cialfi *et al* [44] for fs laser interactions predicts an electron temperature of $T_{\text{hot}} = 1.2$ MeV, which is also consistent with our measurement. Because of the high contrast of the laser pulse there is no significant pre-plasma and electrons are driven into an overdense plasma where they traverse distances greater than the skin depth in less than a laser cycle and thus cannot achieve the full ponderomotive potential. From the known nanowire density determined by scanning electron microscopy and from the fact that the carbon and deuterium atoms are fully ionized, the average plasma electron density is determined to be $n_e = 6.4 \times 10^{22} \text{ cm}^{-3}$. Accounting for a relativistic correction to the plasma frequency this gives a skin depth, $c/\omega_p \approx 80$ nm. For an electron to feel the full ponderomotive potential it needs to oscillate within the field, however in a single half cycle of the laser pulse an electron can gain energy >1 MeV. For $\lambda = 400$ nm the half cycle pulse duration is only 0.67 fs during which a 1 MeV electron will travel ≈ 200 nm into the plasma, a distance far greater than the collisionless skin depth.

In contrast, the nanowire targets allow for the laser pulse to propagate deep into the array, a distance many times greater than the skin depth [24, 25]. This enables electrons to originate from an extended plasma volume greatly increasing the fast electron flux. The data in figure 2 with star markers corresponds to a single shot on a nanowire target has a measured temperature of 4.52 MeV, a $3\times$ increase respect to a solid foil target. In addition to hotter electron temperatures an increase of $22.4\times$ in particle flux is observed compared to the foil targets. Shot to shot variations in the measured temperature for foil targets were within 0.06 MeV (figure 2). More substantial variation was however observed for shots on nanowire targets. For example, the data with square markers yields a hot electron temperature of 2.68 MeV. This fluctuation is attributed to a variation in the number of wires present in the focal spot from shot to shot, as well as local variation in the alignment of the nanowires.

Fully relativistic three-dimension PIC simulations were conducted in order to determine the process of electron acceleration in the nanowire arrays. The wires are rapidly ionized through optical field ionization. Electrons enter gaps between the wires are accelerated towards the substrate by electric field of the laser. A strong electron return current propagates along the length of the wire, which in turn generates a strong azimuthal magnetic field that gives rise to a Lorentz force that pinches the wire [45]. Figures 3(a)–(c) shows the electron density maps plotted in units of critical density ($6.9 \times 10^{21} \text{ cm}^{-3}$) at three different times respect to the arrival of the peak of the laser pulse to the tip of the wires: (a) 35 fs before the peak of the laser pulse reaches the tip of the wires, (b) when the peak of the laser pulse has reached the plane of the tip the nanowire array, and (c) after it has reached the supporting substrate at 35 fs. The wires explode starting from the tips, rapidly filling the gaps between the wires. The corresponding maps of the electric field are plotted in (d)–(f). In (d) the rising edge of the laser pulse penetrates between the wires while the wires themselves are supercritical. By the time the peak reaches the nanowire boundary, (e) plasma has filled the gaps, however the onset of relativistic transparency (RIT) [46, 47] is observed, allowing the laser pulse to continue propagating into the plasma until it encounters the solid density substrate which cannot penetrate (f).

The energy spectrum of electrons which exit the simulation box is shown in figure 3(j). The hot electron temperature from the PIC simulation was found to be $T_{\text{hot}} = 5$ MeV, in good agreement with the experimental measurement in figure 2.

To elucidate the acceleration mechanism, it is useful to follow the trajectory of the most energetic electrons. Figure 4 illustrates the trajectory of several individual electrons which final energy is >15 MeV. The quasi-static electric field that drives the return current accelerates electrons within the wires upwards in the laser backward direction. In addition, electron which leave the nanowire are further accelerated by fields induced by surface waves, as well as the laser. Interaction with the quasi-static magnetic field created by the return current then directs some electrons upwards [45]. The result is that electrons which will reach the highest energies are

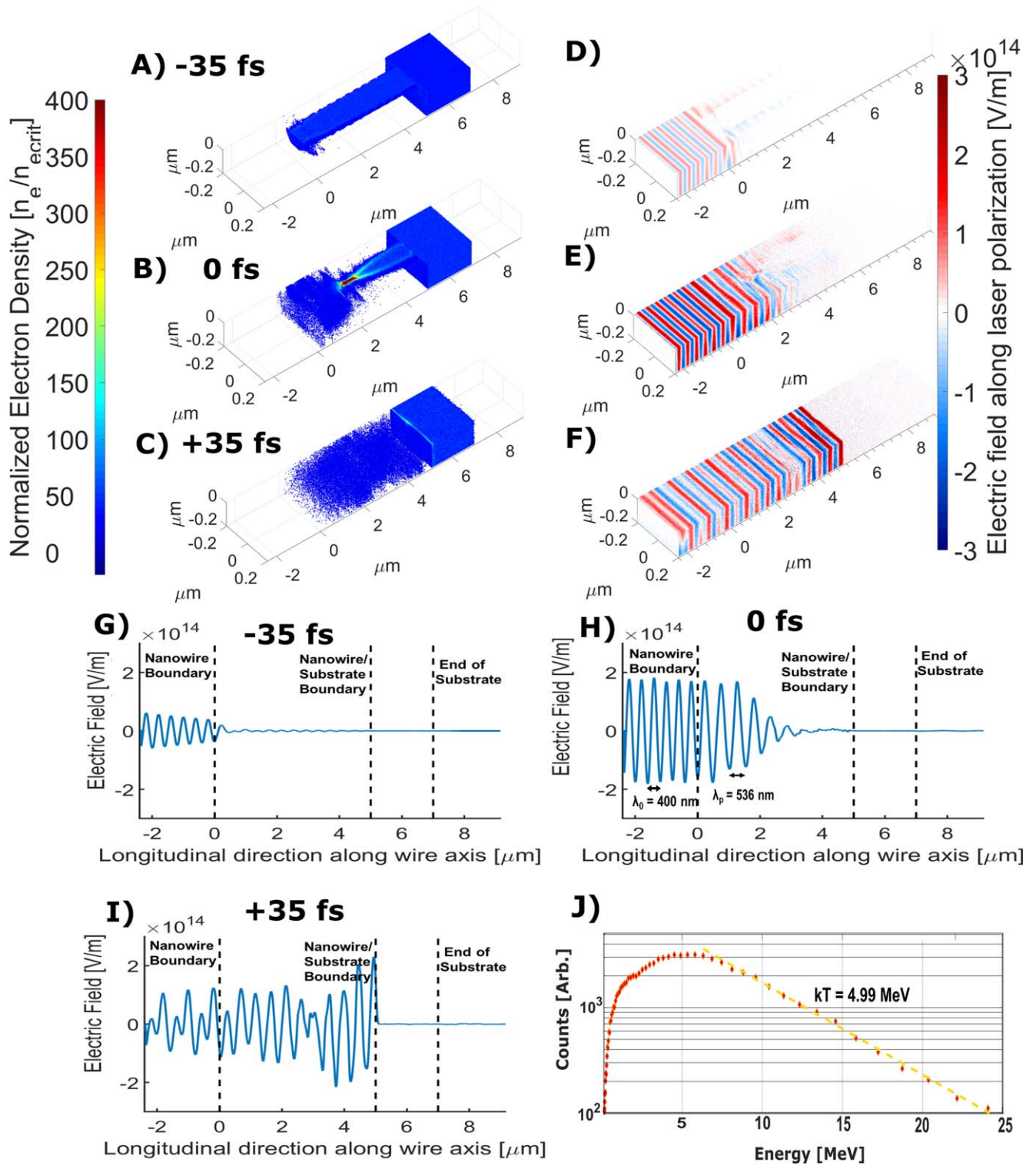


Figure 3. 3D PIC simulations results showing the distribution of the electron density (a)–(c), the electric field (d)–(f) and the 1D plots (g)–(i) of the electric field for three different times, respect to the arrival of the peak of the laser pulse to the plane of the nanowire tips. The 3D visualization has been cut along the nanowire axis to show the center of the nanowire. (j) Synthetic energy spectra of the electrons exiting the simulation though the laser forward face.

originally created anywhere within the nanowires, and undergo a trajectory often interrupted by collision, that predominantly takes them to the plasma near the tip of the wires. Electrons that make it all the way to this lower density plasma

near the vacuum interface are finally stopped by the laser field and by charge separation, reversing their direction. Direct laser acceleration (DLA) in the lower density plasma drives these electrons in the forward direction towards the substrate,

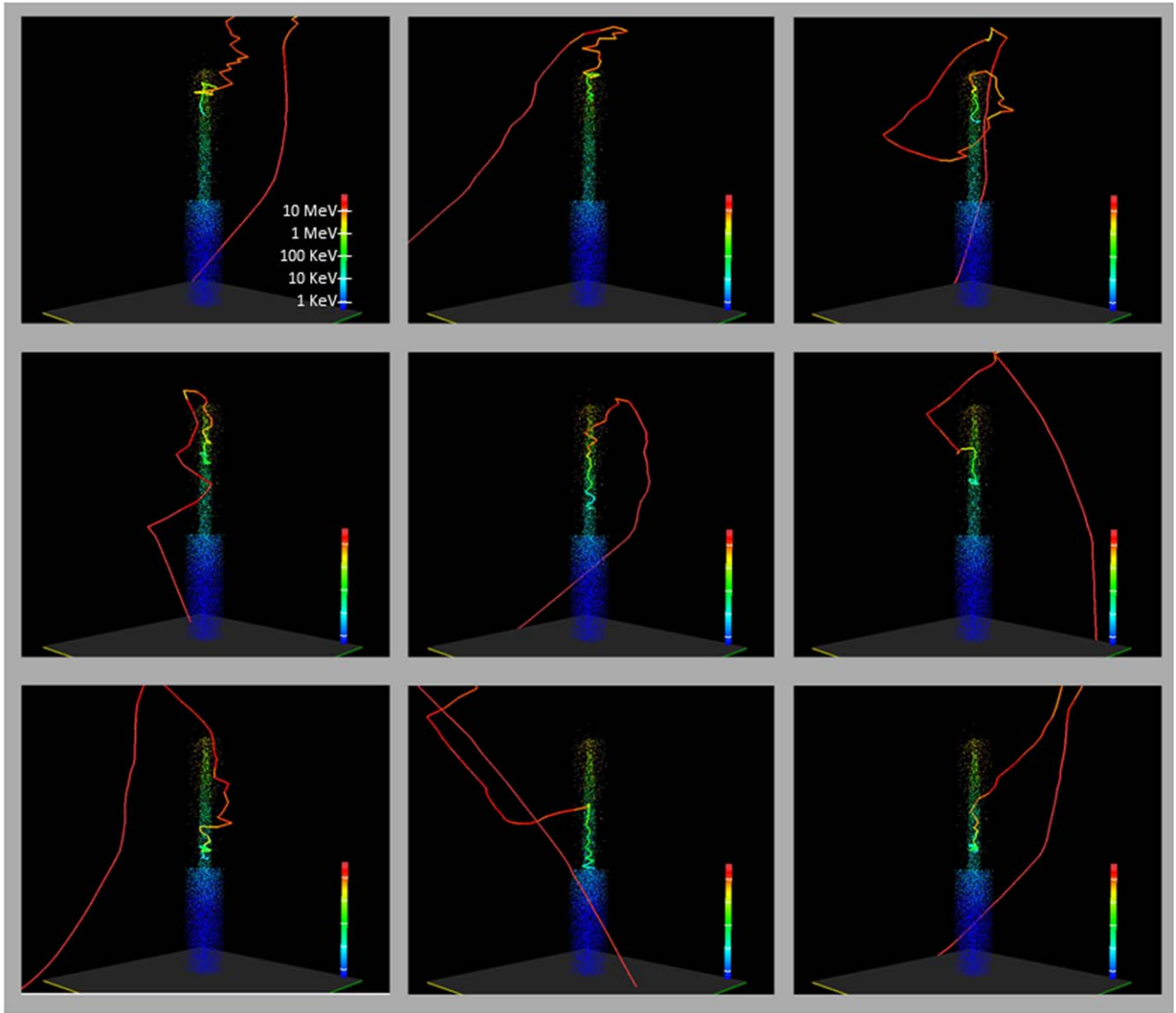


Figure 4. Trajectory of the most energetic electrons in log color scale. Electrons originate within the nanowires where they are accelerated upward by the return current to reach and surpass the tip of the nanowires. There they are strongly accelerated by direct electron acceleration towards the substrate over a distance determined by the de-phasing length between the accelerated electrons and the laser beam. Some of the trajectories are cut by the visualization window used in this illustration. Static images of the nanowires are illustrated for reference. In reality, the wires are evolving in time as the electrons propagate.

where they are partially decelerated [48]. Electrons that make it past the nanowire tip before their motion is reversed are accelerated to the maximum energy. A much larger number of electrons are turned prematurely and accelerated to a lesser energy. Moreover, because electrons generated anywhere in the nanowire volume can be accelerated this results in great increase in the flux of high energy electrons, a $>20\times$ increase respect to foil targets.

The 1D electron phase space is shown in figures 5(a)–(c), where electron bunching at half the laser wavelength is observed, consistent with the DLA mechanism within the low-density plasma region. A steep ramp in the momentum of the electron bunches around the tip of the nanowires is followed by a plateau along the length of the wire. Despite the onset of RIT, DLA is limited to the lower density region of

the plasma. This can be explained by considering the modified dephasing length due to the superluminal phase velocity of the laser within the relativistically transparent plasma. The dephasing length, Δz for an electron being accelerated by DLA is given by: $\Delta z \approx \frac{a_0^2 \lambda_p}{8 R^2}$ where R is the dephasing rate given by: $R = \gamma - \frac{a_0 c}{\sqrt{v_{ph}^2 - c^2}}$ and λ_p is the wavelength in the plasma. This rate is a function of the relativistic critical density through the phase velocity: $v_{ph} = \frac{c}{\sqrt{1 - \frac{n_e}{\gamma n_c}}}$ [49–51].

The phase velocity of the laser while propagating in the dense plasma can be determined directly from the 1D electric field map in figure 4(h) by fitting a sinusoid to the vacuum and plasma regions. The wavelength is measured to increase from $\lambda_0 = 400$ nm in the vacuum to $\lambda_p = 538$ nm in the plasma

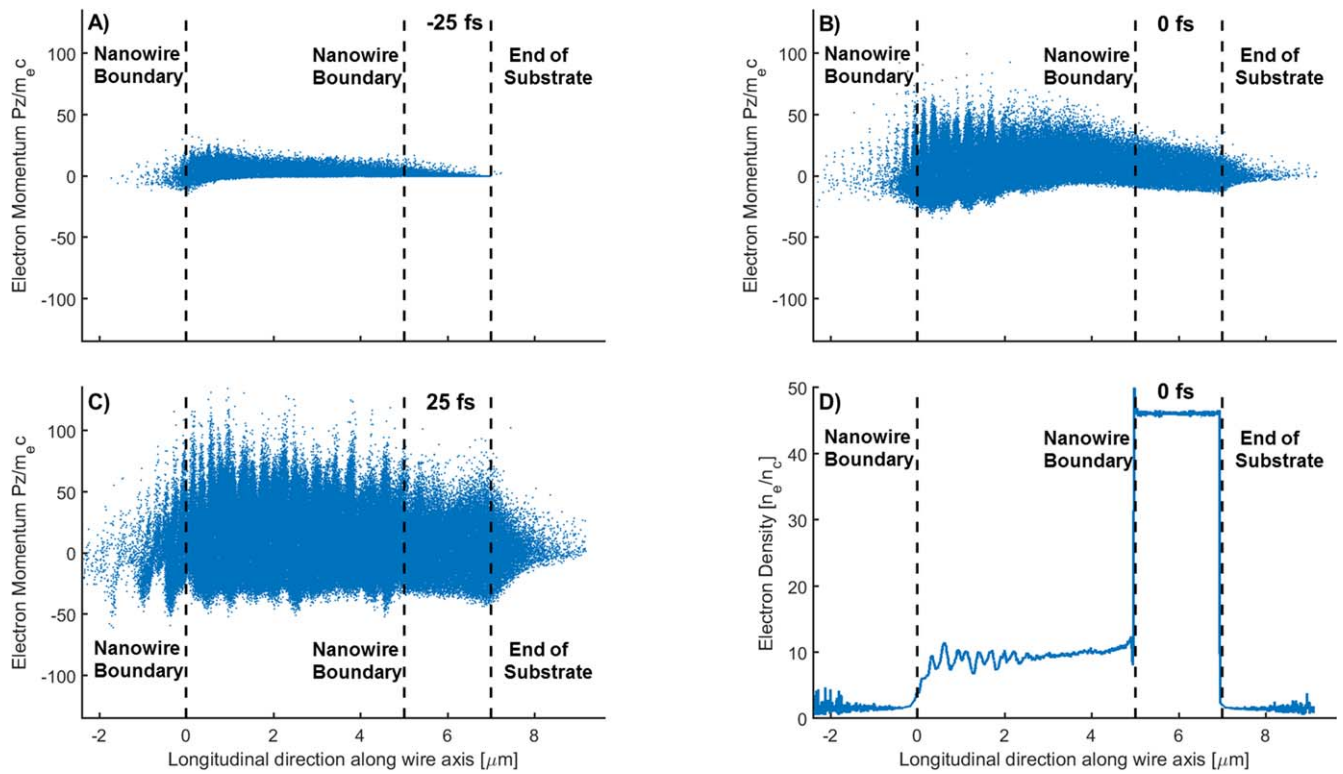


Figure 5. (A) 1D Phase space plots of electron momenta at 25 fs before the peak of the laser pulse reaches the tip of the nanowires and prior to the onset of relativistic transparency. (B) When the peak of the laser has reached the plane of the nanowire boundary. (C) Momenta at 25 fs after the peak of the pulse has reached the nanowires, where it has reached the substrate. (D) Electron density as a function of position when the pulse is at the nanowire boundary (0 fs).

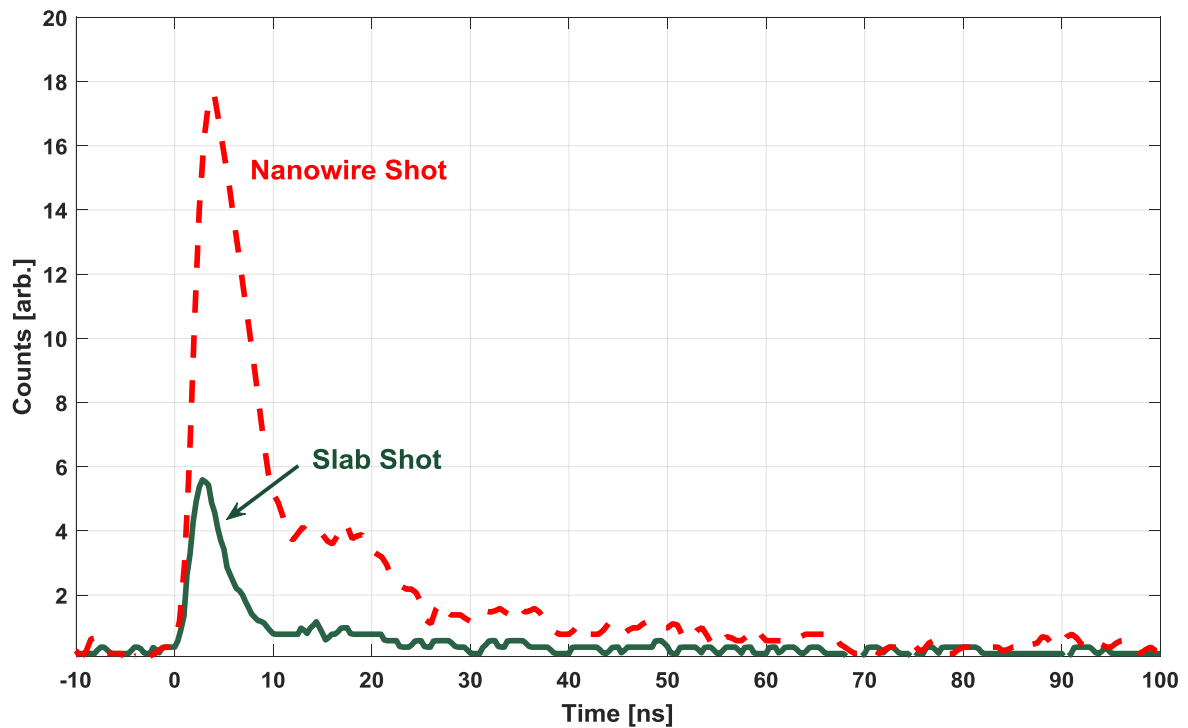


Figure 6. Raw signals from the >1 MeV photon detector indicating a $3.6\times$ enhancement of integrated flux for the nanowire (dashed) over the foil shots (solid). Each curve represents a single shot and all data was collected simultaneously with the electron spectra.

giving a superluminal phase velocity of 1.34 c. Solving for the dephasing length at the simulated $a_0 = 21$, we retrieve a length of $\Delta Z \approx 0.41 \mu\text{m}$. As seen in figure 5(d), a roughly constant electron density, $n_e \approx 10 n_c$ is present in the nanowire plasma. This density is below the threshold of RIT that occurs at $\approx 15 n_c$. In contrast, at the tip of the wire the density is much lower, allowing for DLA without dephasing. This indicates that if the objective is to further gain energy, targets must be designed with lower densities. In such a scenario, electrons could continue to gain energy over a longer distance, increasing the hot electron temperature.

One noteworthy result of this enhancement in high energy electron energy and flux is the increased generation of MeV bremsstrahlung photons. The scintillator/photomultiplier detector was deployed to monitor the emission of photons with $>1 \text{ MeV}$ simultaneously with the electron spectra. In figure 6, data corresponding to the brightest shot on foil targets is shown with continuous lines while the dashed lines correspond to the brightest nanowire shot. We measure a $3.6\times$ enhancement in the integrated signal for the nanowire target over the foil target. This measurement shows that the enhanced electron acceleration from nanostructured targets are of interest for the implementation of a bright MeV secondary photon source. To further increase the brightness a high-Z converter could be placed at the target rear in a pitcher-catcher configuration.

In addition to boosted gamma ray production this electron acceleration mechanism is likely to translate to enhanced ion acceleration. Higher energy and flux of deuterium ions and protons were measured at $8 \times 10^{19} \text{ W cm}^{-2}$ with the same targets [27], and it is expected that at the intensity of this experiment, ions would be similarly accelerated in an enhanced TNSA mechanism.

4. Conclusion


In summary, we report a significant enhancement in both the energy and flux of high energy electrons in sub-wavelength aligned low Z nanowire targets irradiated by ultrahigh contrast pulses of highly relativistic intensities. We report greatly increased ($22.4\times$) electron flux in comparison to foil targets of the same material, CD_2 , as well as a $3\times$ increase in the hot electron temperature. Electrons originating from the nanowires undergo a complex trajectory in which they are first accelerated in the laser backward direction to reach the lower density plasma region near the tip of the nanowires, where the field of laser along with quasi-static fields due to charge separation stops their motion and reverse their direction. The electrons are subsequently accelerated by direct electron acceleration until they outrun the laser pulse. The experimental results also show a significant increase ($3.6\times$) in the flux of $>1 \text{ MeV}$ photons generated by bremsstrahlung, suggesting such aligned nanostructure targets have potential application in the development of high brightness, short pulse duration, multi-MeV x-ray secondary sources when used in a pitcher-catcher configuration.

Acknowledgments

This material is based on work supported by the Air Force Office of Scientific Research under award number FA9550-17-1-0278. The simulations were conducted using the CU-CSU Summit High Performance Computer System, NSF (ACI-1532235). We acknowledge the help of Timothy Kaiser in running the PIC code on the CU-SCU Summit High Performance Computer System. All data are available from the authors upon request.

ORCID iDs

A Moreau  <https://orcid.org/0000-0002-3266-3461>

M G Capeluto  <https://orcid.org/0000-0002-9569-6076>

References

- [1] Wharton K B, Hatchett S P, Wilks S C, Key M H, Moody J D, Yanovsky V, Offenberger A A, Hammel B A, Perry M D and Joshi C 1998 Experimental measurements of hot electrons generated by ultraintense ($>10^{19} \text{ W cm}^{-2}$) laser-plasma interactions on solid-density targets *Phys. Rev. Lett.* **81** 822–5
- [2] Macchi A, Borghesi M and Passoni M 2013 Ion acceleration by superintense laser-plasma interaction *Rev. Mod. Phys.* **85** 751–93
- [3] Badziak J 2018 Laser-driven ion acceleration: methods, challenges and prospects *J. Phys.: Conf. Ser.* **959** 012001
- [4] Yin L, Albright B J, Hegelich B M, Bowers K J, Flippo K A, Kwan T J and Fernández J C 2007 Monoenergetic and GeV ion acceleration from the laser breakout afterburner using ultrathin targets *Phys. Plasmas* **14** 056705
- [5] Habara H *et al* 2004 Ion acceleration from the shock front induced by hole boring in ultraintense laser-plasma interactions *Phys. Rev. E* **70** 4
- [6] Snavely R A *et al* 2000 Intense high-energy proton beams from petawatt-laser irradiation of solids *Phys. Rev. Lett.* **85** 2945–8
- [7] Poole P L *et al* 2018 Laser-driven ion acceleration via target normal sheath acceleration in the relativistic transparency regime *New J. Phys.* **20** 013019
- [8] Yan Y, Wu Y, Chen J, Yu M, Dong K and Gu Y 2017 Positron acceleration by sheath field in ultra-intense laser-solid interactions *Plasma Phys. Control. Fusion* **59** 045015
- [9] Williams G J *et al* 2016 Target material dependence of positron generation from high intensity laser-matter interactions *Phys. Plasmas* **23** 123109
- [10] Chen H *et al* 2015 Scaling the yield of laser-driven electron-positron jets to laboratory astrophysical applications *Phys. Rev. Lett.* **114** 215001
- [11] Palaniyappan S *et al* 2018 MeV bremsstrahlung x rays from intense laser interaction with solid foils *Laser Part. Beams* **36** 502–6
- [12] Perry M D, Sefcik J A, Cowan T, Hatchett S, Hunt A, Moran M, Pennington D, Snavely R and Wilks S C 2002 Hard x-ray production from high intensity laser solid interactions (invited) *Rev. Sci. Instrum.* **70** 265–9
- [13] Chen H *et al* 2017 High-energy ($>70 \text{ keV}$) x-ray conversion efficiency measurement on the ARC laser at the National Ignition Facility *Phys. Plasmas* **24** 033112

- [14] Andreev A A and Platonov K Y 2016 X-ray generation by fast electrons propagating in nanofibres irradiated by a laser pulse of relativistic intensity *Quantum Electron.* **46** 109–18
- [15] Murnane M M, Kapteyn H C, Gordon S P, Bokor J, Glytsis E N and Falcone R W 1993 Efficient coupling of high-intensity subpicosecond laser pulses into solids *Appl. Phys. Lett.* **62** 1068–70
- [16] Khattak F Y *et al* 2005 Enhanced He- α emission from ‘smoked’ Ti targets irradiated with 400 nm, 45 fs laser pulses *Europhys. Lett.* **72** 242–8
- [17] Kulcsár G, Almawlawi D, Budnik F W, Herman P R, Moskovits M, Zhao L and Marjoribanks R S 2000 Intense picosecond x-ray pulses from laser plasmas by use of nanostructured ‘Velvet’ targets *Phys. Rev. Lett.* **84** 5149–210
- [18] Mondal S *et al* 2011 Highly enhanced hard x-ray emission from oriented metal nanorod arrays excited by intense femtosecond laser pulses *Phys. Rev. B* **83** 035408
- [19] Ovchinnikov A, Kostenko O, Chefonov O, Rosmej O, Andreev N, Agranat M, Duan J, Liu J and Fortov V 2011 Characteristic x-rays generation under the action of femtosecond laser pulses on nano-structured targets *Laser Part. Beams* **29** 249–54
- [20] Nishikawa T, Suzuki S, Watanabe Y, Zhou O and Nakano H 2004 Applied physics B Efficient water-window x-ray pulse generation from femtosecond-laser-produced plasma by using a carbon nanotube target *Lasers Opt.* **78** 885–90
- [21] Gordon S P, Donnelly T, Sullivan A, Hamster H and Falcone R W 1994 X rays from microstructured targets heated by femtosecond lasers *Opt. Lett.* **19** 484
- [22] Rajeev P P, Taneja P, Ayyub P, Sandhu A S and Kumar G R 2003 Metal nanoplasmas as bright sources of hard x-ray pulses *Phys. Rev. Lett.* **90** 115002
- [23] Sumeruk H A, Kneip S, Symes D R, Churina I V, Belolipetski A V, Donnelly T D and Ditmire T 2007 Control of strong-laser-field coupling to electrons in solid targets with wavelength-scale spheres *Phys. Rev. Lett.* **98** 045001
- [24] Purvis M A *et al* 2013 Relativistic plasma nanophotonics for ultrahigh energy density physics *Nat. Photon.* **7** 796–800
- [25] Bargsten C *et al* 2017 Energy penetration into arrays of aligned nanowires irradiated with relativistic intensities: scaling to terabar pressures *Sci. Adv.* **3** e1601558
- [26] Hollinger R *et al* 2017 Efficient picosecond x-ray pulse generation from plasmas in the radiation dominated regime *Optica* **4** 1344
- [27] Curtis A *et al* 2018 Micro-scale fusion in dense relativistic nanowire array plasmas *Nat. Commun.* **9** 1077
- [28] Chatterjee G *et al* 2012 Macroscopic transport of mega-ampere electron currents in aligned carbon-nanotube arrays *Phys. Rev. Lett.* **108** 235005
- [29] Snyder J *et al* 2019 Relativistic laser driven electron accelerator using micro-channel plasma targets *Phys. Plasmas* **26** 033110
- [30] Cristoforetti G *et al* 2017 Transition from coherent to stochastic electron heating in ultrashort relativistic laser interaction with structured targets *OPEN Sci. Rep.* **7** 1479
- [31] Jiang S *et al* 2016 Microengineering laser plasma interactions at relativistic intensities *Phys. Rev. Lett.* **116** 085002
- [32] Khaghani D *et al* 2017 Enhancing laser-driven proton acceleration by using micro-pillar arrays at high drive energy *Sci. Rep.* **7** 11366
- [33] Sarkar D *et al* 2017 Silicon nanowire based high brightness, pulsed relativistic electron source *APL Photonics* **2** 066105
- [34] Andreev A A, Nickles P V and Platonov K Y 2014 Generation and transport of energetic electrons in nanowire targets irradiated by relativistic intense laser pulses *Plasma Phys. Contr. Fusion* **56** 084005
- [35] Andreev A A and Platonov K Y 2014 Generation, transport, and focusing of fast electrons in nanofilaments of a target irradiated by a short laser pulse with ultrarelativistic intensity *JETP Lett.* **98** 790–5
- [36] Wang Y, Wang S, Rockwood A, Luther B M, Hollinger R, Curtis A, Calvi C, Menoni C S and Rocca J J 2017 085 PW laser operation at 33 Hz and high-contrast ultrahigh-intensity $\lambda = 400$ nm second-harmonic beamline *Opt. Lett.* **42** 3828
- [37] Williams G J, Maddox B R, Chen H, Kojima S and Millecchia M 2014 Calibration and equivalency analysis of image plate scanners *Citation: Rev. Sci. Instrum.* **85** 11–604
- [38] Dahl D A *SIMION 3D, 8.1 ed.* Idaho National Engineering and Environmental Laboratory
- [39] Dubois J L *et al* 2014 Target charging in short-pulse-laser-plasma experiments *Phys. Rev. E* **89** 013102
- [40] Cowan T E *et al* 2000 High energy electrons, positrons and photonuclear reactions in petawatt laser-solid experiments *High-Field Science* ed T Tajima *et al* (Boston, MA: Springer US) pp 145–56
- [41] Cobble J A, Palaniyappan S, Johnson R P, Shimada T, Huang C, Gautier D C, Clark D D, Falk K and Jung D 2016 Laser-driven micro-Coulomb charge movement and energy conversion to relativistic electrons *Phys. Plasmas* **23** 093113
- [42] Pukhov A 1999 Three-dimensional electromagnetic relativistic particle-in-cell code VLPL (Virtual Laser Plasma Lab) *J. Plasma Phys.* **61** 425–33
- [43] Beg F N, Bell A R, Dangor A E, Danson C N, Fews A P, Glinesky M E, Hammel B A, Lee P, Norreys P A and Tatarakis M 1997 A study of picosecond laser-solid interactions up to 10^{19} W cm⁻² *Phys. Plasmas* **4** 447–57
- [44] Cialfi L, Fedeli L and Passoni M 2016 Electron heating in subpicosecond laser interaction with overdense and near-critical plasmas *Phys. Rev. E* **94** 053201
- [45] Kaymak V, Pukhov A, Shlyaptsev V N and Rocca J J 2016 Nanoscale ultradense Z-pinch formation from laser-irradiated nanowire arrays *Phys. Rev. Lett.* **117** 035004
- [46] Fernández J C *et al* 2017 Laser-plasmas in the relativistic-transparency regime: science and applications *Phys. Plasmas* **24** 056702
- [47] Palaniyappan S *et al* 2012 Dynamics of relativistic transparency and optical shuttering in expanding overdense plasmas *Nat. Phys.* **8** 763–9
- [48] Pukhov A, Sheng Z M and Meyer-ter-Vehn J 1999 Particle acceleration in relativistic laser channels *Phys. Plasmas* **6** 2847–54
- [49] Arefiev A V, Robinson A P and Khudik V N 2015 Novel aspects of direct laser acceleration of relativistic electrons *J. Plasma Phys.* **81** 475810404
- [50] Arefiev A V, Khudik V N, Robinson A P, Shvets G, Willingale L and Schollmeier M 2016 Beyond the ponderomotive limit: direct laser acceleration of relativistic electrons in sub-critical plasmas *Phys. Plasmas* **23** 056704
- [51] Robinson A P, Arefiev A V and Khudik V N 2015 The effect of superluminal phase velocity on electron acceleration in a powerful electromagnetic wave *Phys. Plasmas* **22** 083114